Inorganic Chemistry
Article
Cite This: Inorg. Chem. XXXX, XXX, XXX−XXX
pubs.acs.org/IC

H_2hox: Dual-Channel Oxine-Derived Acyclic Chelating Ligand for ^{68}Ga Radiopharmaceuticals

Xiaozhu Wang,[†] María de Guadalupe Jaraquemada-Peláez,[†] Yang Cao,[†] Jinhe Pan,[‡] Kuo-Shyan Lin,[‡] Brian O. Patrick,[†] and Chris Orvig*[,†]

[†]Medicinal Inorganic Chemistry Group, Department of Chemistry, University of British Columbia, 2036 Main Mall, Vancouver, British Columbia V6T 1Z1, Canada

[‡]BC Cancer Agency, 675 West 10th Avenue, Vancouver, British Columbia V5Z 1L3, Canada

Supporting Information

ABSTRACT: An acyclic hexadentate oxine-derived chelating ligand, H_2hox, was investigated as an alternative to current chelators for ^{68}Ga. The straightforward preparation of H_2hox, involving only one or two steps, obviates the synthetic challenges associated with many reported ^{68}Ga chelators; it forms a Ga^{3+} complex of great stability (log K = 34.4) with a remarkably high gallium scavenging ability ($pGa^{3+} = -\log[Ga^{3+}_{free}] = 28.3$, ($[Ga^{3+}] = 1\ \mu M$; $[L^{x-}] = 10\ \mu M$; pH 7.4, and 25 °C)). Moreover, H_2hox coordinates ^{68}Ga quantitatively in 5 min at room temperature in ligand concentrations as low as 1×10^{-7} M, achieving an unprecedented high molar activity of 11 ± 1 mCi/nmol (407 ± 3.7 MBq/nmol) without purification, suggesting prospective kit-based convenience. $[^{68}Ga(hox)]^+$ showed no decomposition in a plasma challenge. Good in vivo stability and fast renal and hepatic clearance of the $[^{68}Ga(hox)]^+$ complex were demonstrated using dynamic positron emission tomography/computed tomography imaging. The intrinsic fluorescence of $[Ga(hox)]^+$ allowed for direct fluorescence imaging of cellular uptake and distribution, demonstrating the dual-channel detectability and intracellular stability of the metal complex.

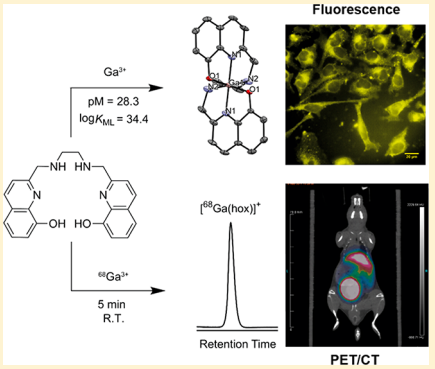

INTRODUCTION

The ^{68}Ge/^{68}Ga generator system is one of the most attractive systems for diagnostic nuclear medicine. It could be utilized for an extended period due to the 271 d half-life of the parent isotope ^{68}Ge. The daughter isotope ^{68}Ga has a high positron decay yield (89%, 1.899 keV) and a relatively short half-life time ($t_{1/2}$ = 68 min), and it is becoming increasingly important as a versatile and easily available positron emission tomography (PET) imaging tracer.[1−3]

Because of the ^{68}Ga short half-life, an ideal chelating ligand should rapidly achieve efficient and reproducible radiolabeling under mild conditions (room temperature (RT) and near neutral pH), yielding a stable radiopharmaceutical with high molar activity at low concentration that could be used in routine clinical practice without further purification. Thus, such a radiopharmaceutical ligand would be ideal for the development of a toolkit for convenient clinical use.[4−7] The macrocyclic chelator 1,4,7,10-tetraazacyclododecane-1,4,7,10-tetraacetic acid (DOTA; Scheme 1) is the most commonly used chelator for ^{68}Ga labeling.[8−12] The preorganized closed chain structure guarantees a high kinetic inertness and thermodynamic stability; however, concomitant are longer labeling time and high temperature, which is incompatible with the labeling of thermally sensitive biovectors. Moreover, the synthesis of those cyclic chelators and corresponding bifunctional derivatives is also challenging and expensive involving postsynthetic purification steps and workup for the removal of impurities.[13]

Over the past decade, several Ga^{3+} chelators have been developed to overcome these drawbacks including 1,4,7-triazacyclononane-1,4,7-triacetic acid (NOTA),[14,15] NOTP,[16] TRAP,[17,18] DATA,[19−21] PCTA,[22] HBED,[23−25] and (1,2-[[6-carboxypyridin-2-yl]methylamino]-ethane (H_2dedpa)[1,26−32] (Scheme 1). NOTA radiolabels Ga^{3+} at RT in 10 min at pH 3−5.5.[14] NOTP and TRAP, the triphosphate analogues of NOTA, could be used in a broader pH range, especially at lower pH.[16,33] HBED and its bioconjugate showed a high thermodynamic stability and serum stability.[23] THP achieved a 97% radiochemical yield at 0.5 μM and near neutral pH,[7] and finally H_2dedpa can obtain a quantitative radiochemical yield at concentrations as low as 0.1 μM.[27]

There are still limitations among those chelators. For example, the labeling performance of NOTA and TRAP at near-physiological pH is not as good as at lower pH and requires higher concentrations; HBED forms multiple species in solution with Ga^{3+}, and thus, it is not ideal for quick and easy purification and kit-based application.[7] The synthesis of THP and its derivative are nontrivial.[19] Synthetic accessibility

Received: May 3, 2018

DOI: 10.1021/acs.inorgchem.8b01208
Inorg. Chem. XXXX, XXX, XXX−XXX

Scheme 1. Examples of Chelating Ligands for Ga^{3+} from the Literature

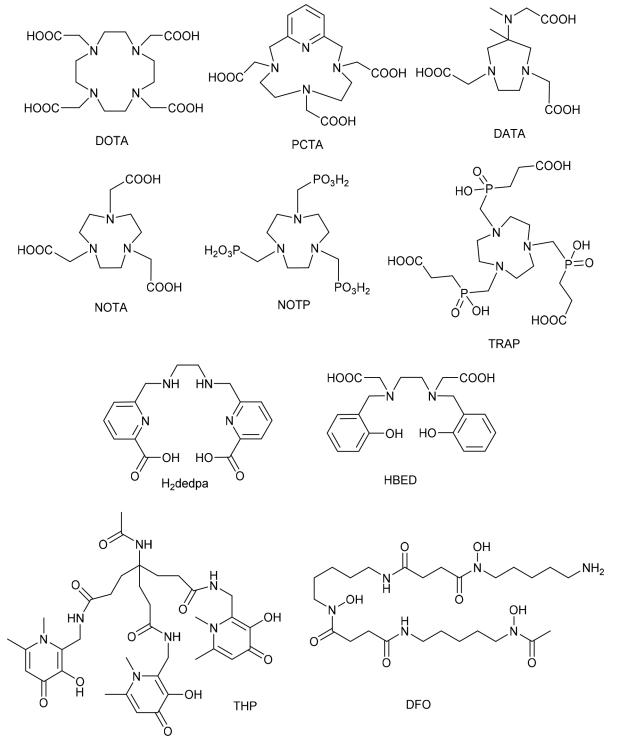

is also a challenge for H_2dedpa and most of the cyclic chelators as well.[27]

In this work, we report a tightly binding acyclic hexadentate chelator that will certainly be applicable to ^{68}Ga PET imaging: H_2hox with rigid "bis-ox" (8-hydroxyquinoline) arms (Scheme 2). The synthesis of H_2hox is easy and fast (one or two steps),

Scheme 2. Design Paradigm for H_2hox

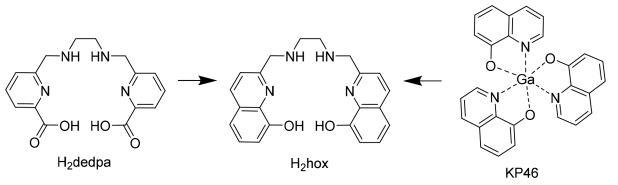

and solution studies reveal the presence of a single complex species in a broad pH range (1−11) with higher log K_{ML} (34.4) and pM value (28.3) than for most of the Ga^{3+} chelators. H_2hox showed fast and quantitative ^{68}Ga complexation at mild conditions (5 min, RT) with a concentration as low as 1×10^{-7} M and an unprecedented high molar activity without purification. Plasma challenge experiments and dynamic PET imaging confirm excellent in vitro and in vivo stability. These characteristics suggest strong relevance to toolkit radiopharmaceuticals ("shake and shoot"); to complement these ideal properties, the florescence of the chelating ligand is turned on by complexation to Ga^{3+}, and this was used to investigate the cellular distribution of $[Ga(hox)]^+$ directly and showed the potential for dual-channel or bimodal imaging.

RESULTS AND DISCUSSION

Our group has screened many acyclic chelators for gallium radiolabeling in the past decade, and H_2dedpa was the most successful, showing fast chelation and high stability, properties close to those of DOTA and NOTA, until we discovered H_2hox.[27,34−38] The high stability of H_2dedpa was attributed to a nearly perfect size fit and geometric arrangement of coordination atom and bonds. Oxine (8-hydroquinoline), the bidentate ligand in the anticancer compound KP46, possesses a very high stability constant for its 3:1 complex with gallium ($\log \beta_{ML_3} = 36.4$).[39] In the design of our second generation of acyclic chelators for gallium, a combination of the respective advantages of H_2dedpa and oxine was sought, leading to the structure of H_2hox (Scheme 2).

Synthesis and Characterization. The only previous report of H_2hox was in 1972 by Hata and Uno[40,41] as an analytical reagent (BHQED) for divalent metals, and it has not been further explored in the intervening near-half-century; however, Hata and Uno's synthetic protocol was difficult to reproduce, resulting in low yield and purity. Thus, a modified synthetic route was developed (Scheme 3). 8-Hydroxyquinoline-2-aldehyde is a cheap starting material purchased from a commercial supplier or synthesized from 2-methyl-8-hydroxyquinoline in one step without protection. H_2hox was synthesized by reductive amination of 8-hydroxyquinoline-2-aldehyde and ethylenediamine (en) in one step and purified by recrystallization to obtain 87% yield without the need of column separation. In the Hata and Uno synthetic protocol, most of the product precursor was filtered out and discarded before the reaction was quenched with acetic acid, giving a low yield. Therefore, in our new protocol the reaction was quenched by HCl directly, and the product precipitated out in high yield after the pH was adjusted to neutral. The new route takes only one or two steps (depending on starting material), quickly and economically yielding grams of ligand. This is particularly notable when comparing with most of the previously reported ligands such as NOTA, DOTA, TRAP, NOTP, DATA, THP, and H_2dedpa. Moreover, in work to be published subsequently, we can conveniently form a bifunctional version by using a functionalized diamine backbone (e.g., (4-nitrobenzyl)ethylenediamine). The bifunctional tracer and the hydrophilicity tuning can be achieved by direct modification on the aromatic ring; this has been widely used in the 8-hydroquinoline-based pharmaceuticals and in organic light emitting diode (OLED) agents.[42−46] The tedious and challenging synthesis and purification of most of the previous chelators is a significant barrier to commercial applicability. H_2hox overcomes this barrier and is ideally suited for real clinical research and wide application.

Scheme 3. Synthesis of H_2hox[a]

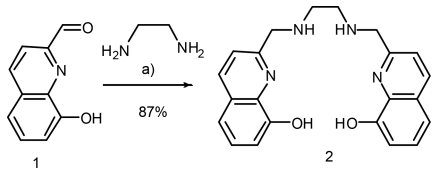

[a](a) Ethylenediamine, CH_3CH_2OH, at 60°C, 4 h; CH_3CH_2OH, $NaBH_4$ (5 equiv), overnight.

X-ray Crystallography and DFT Calculations. The structure of H_2hox was confirmed by X-ray diffraction data using a suitable crystal obtained by recrystallization from methanol. Two crystallographically independent structures, both with C_i symmetry (Figure S7), were identified featuring

DOI: 10.1021/acs.inorgchem.8b01208
Inorg. Chem. XXXX, XXX, XXX−XXX

two 8-hydroxyquinoline moieties connected to an ethylenediamine backbone giving rise to six potential coordination sites (Figure 1a). [Ga(hox)][ClO_4] crystals were obtained by layer

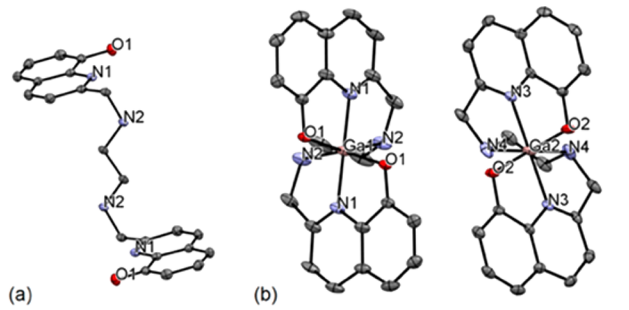

Figure 1. ORTEP diagrams of (a) one of the two crystallographically independent structures of H_2hox, and (b) two crystallographically independent cations of [Ga(hox)] [ClO_4]; thermal ellipsoids shown at 50% probability level; hydrogen atoms and solvent acetonitrile molecules omitted for clarity.

diffusion of diethyl ether into a dichloromethane solution of the complex, and the material crystallizes with two C_i symmetric structures (Figure 1b). Selected bond parameters of the mer-[Ga(hox)]$^+$ cation are summarized in Table 1 and

Table 1. Selected Bond Distances in the Cations [Ga(hox)]$^+$ and [Ga(dedpa)]$^+$

[Ga(hox)]$^+$			[Ga(dedpa)]$^+$ [a]		
atom	atom	length (Å)	atom	atom	length (Å)
Ga1	O11	1.959	Ga1	O11	1.970
Ga1	O1	1.959	Ga1	O1	1.982
Ga1	N1	1.982	Ga1	N1	1.986
Ga1	N11	1.982	Ga1	N11	1.989
Ga1	N21	2.190	Ga1	N21	2.112
Ga1	N2	2.190	Ga1	N2	2.113

[a]From ref 27; pyr = pyridine, and en = ethylenediamine.

compared to those of mer-[Ga(dedpa)]$^+$. The meridional arrangement of the six-coordinating atoms in [Ga(hox)]$^+$ is similar to that in [Ga(dedpa)]$^+$; however, in [Ga(hox)]$^+$, the Ga−O and Ga−N(pyr) bonds are slightly shorter, while Ga−N(en) bonds are longer. The evenly distributed array of bond lengths suggests an excellent fit of [hox]$^{2-}$ with the Ga^{3+} cation and a stability possibly comparable to that of [dedpa]$^{2-}$ (for further structural data see the Supporting Information).

The coordination geometries of the [Ga(dedpa)]$^+$ and [Ga(hox)]$^+$ cations in aqueous solution were simulated using density functional theory (DFT); Figure 2a,b. The calculated bond parameters of these two cations are summarized in Tables S5 and S6 and compared with their solid-state structures. Similar geometries and bond lengths are observed in the simulated solution structures of both cations. The corresponding molecular electrostatic potential mapping (MEP) of these geometries is shown in Figure 2c,d. In the [Ga(hox)]$^+$ cation, less prominent electronegative potential (indicated by red areas) is observed, which could result in a higher stability and a slower rate of hydrolysis of [Ga(hox)]$^+$ compared to that of [Ga(dedpa)]$^+$ under acidic conditions. Moreover, a more evenly distributed surface charge would translate into a higher lipophilicity for [Ga(hox)]$^+$ versus [Ga(dedpa)]$^+$.

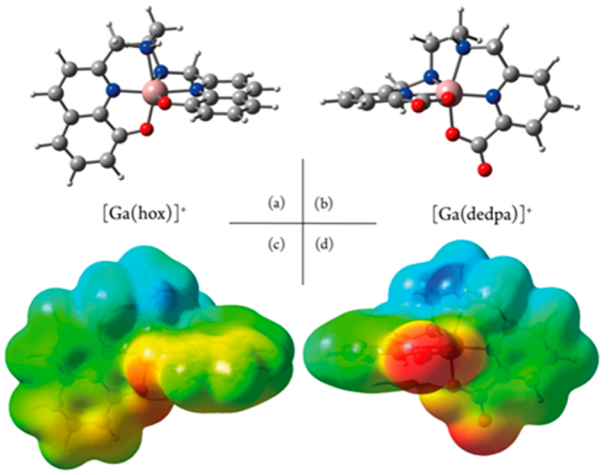

Figure 2. DFT-optimized structures of the (a) [Ga(hox)]$^+$ and (b) [Ga(dedpa)]$^+$ cations with hexacoordinated metal centers, and the electrostatic potentials of (c) [Ga(hox)]$^+$ and (d) [Ga(dedpa)]$^+$ mapped onto their electron density. The MEP represents a maximum potential of 0.25 au and a minimum of −0.02 au mapped onto electron density isosurface (0.002 e Å^{-3}, red to blue = negative to positive).

Solution Thermodynamics. High thermodynamic stability (log K_{ML}) and kinetic inertness are required for in vivo application of radiopharmaceutical metal complexes, to minimize transchelation and transmetalation reactions caused by endogenous ligands and metals. The stepwise protonation constants of H_2hox included in the calculation of the log K_{ML} were determined by UV in batch spectrophotometric titrations, as the pH-potentiometric method was unsuitable because of the insufficient solubility of H_2hox. The spectral data were refined using the HypSpec2014 program (Table 2).[47]

Table 2. Protonation Constants of H_2hox at 25°C

equilibium	log β	log K	log K[a]
$L + H^+ \leftrightarrows HL$	10.88(1)[b]	10.88	11.35
$HL + H^+ \leftrightarrows H_2L$	20.69(1)[b]	9.81[b]	10.81
$H_2L + H^+ \leftrightarrows H_3L$	29.08(1)[b]	8.39[b]	8.15
$H_3L + H^+ \leftrightarrows H_4L$	35.14(2)[b]	6.06[b]	5.12
$H_4L + H^+ \leftrightarrows H_5L$	35.78(6)[c]	0.64[c]	ND
$H_5L + H^+ \leftrightarrows H_6L$	36.02(8)[c]	0.24[c]	ND

[a]From ref 40, 50 v/v % aqueous dioxane solution, I = 0.1 M KCl. Charges are omitted for clarity, ND = not determined. [b]This work, I = 0.16 M NaCl. [c]This work, not evaluated at constant I = 0.16 M NaCl.

H_2hox in its neutral form is denoted as H_2L, whereas its fully protonated form in very acidic solution is H_6L^{4+}. The latter possesses six potential protonation sites: two phenolate oxygen atoms, two pyridyl nitrogen atoms, and the two secondary amine nitrogen atoms on the en backbone. Hata and Uno determined and assigned the first four protonation constants of H_2hox by pH-potentiometric titrations in a H_2O−dioxane solvent mixture (50% v/v, μ = 0.1 M KCl, 25 °C) due to its insufficient solubility in water.[40,41] In this work, we were able to analyze all six protonation events in water by exhaustive UV spectrophotometric titrations, taking advantage of the high and different molar absorptivities of each protonated species of H_2hox. These titrations were performed from very acidic solutions until pH 11.80, showing well-defined isosbestic points (Figure S1a−f) indicative of consecutive deprotonation

DOI: 10.1021/acs.inorgchem.8b01208
Inorg. Chem. XXXX, XXX, XXX−XXX

steps of the ligand. Seven absorbing species were identified (Figure S2); six protonation constants were determined using the HypSpec2014 program[47] and summarized in Table 2. The distribution diagram is presented in Figure 3a.

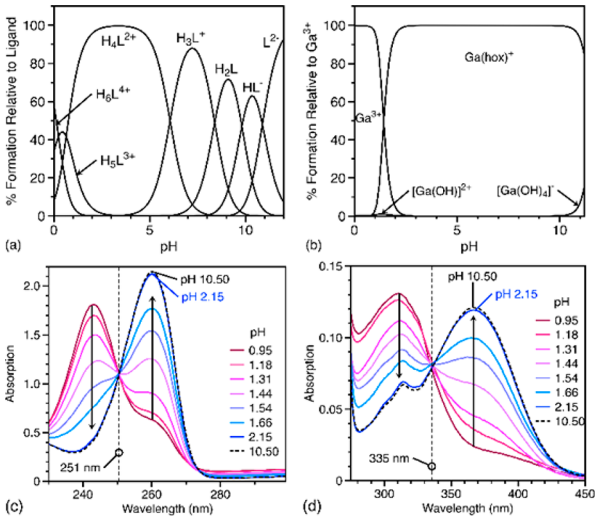

Figure 3. (a) Distribution diagram of H_2hox calculated using the protonation constants in Table S1, at ligand concentration of 2.72 × 10^{-5} M. (b) Distribution diagram of the Ga-hox system, $[Ga]^{3+}$ = $[H_2hox]$ = 2.82 × 10^{-5} M; 25 °C; I = 0.16 M NaCl. (c, d) Representative spectra in the batch UV spectrophotometric titration of the Ga^{3+}-H_2hox system, 1:1 metal-to-ligand molar ratio, $[H_2hox]$ = 2.82 × 10^{-5} M, (l = 1 cm) at 0.16 M NaCl and 25 °C.

From the analysis of the spectra of H_2hox solutions between pH 0−3.39 (Figure S1a,b), the ligand at its fully protonated form H_6L^{4+} presents similar spectroscopic features to those of fully protonated oxine ($H_2L_{ox}^{+}$) reported by both Choppin[48] and Enyedy,[39] with almost doubled molar absorptivities for λ_{max} = 260 and 378 nm consistent with two protonated quinolinium-NH^{+} chromophores (Table S1). The H_6L^{4+} species transforms into the H_5L^{3+} species with the appearance of isosbestic points at 249 and 346 nm, which have been reported also for the deprotonation of $H_2L_{ox}^{+}$ (Table S1). The molar absorptivities for the H_5L^{3+} species are of the same order of magnitude as those of the fully protonated oxine ($H_2L_{ox}^{+}$), consistent with one protonated quinolinium-NH^{+}. This allows for the assignment of the two most acidic pK_a values to the dissociation of the protons from the two quinoline nitrogen atoms (pK_1 = 0.24(8) and pK_2 = 0.64(6)). In addition, the spectra of the species HL^{-} and L^{2-} in most basic conditions show spectroscopic evolution similar to that observed for the quinolinate species of oxine (L_{ox}^{-}), with the appearance of isosbestic points at 249 and 320 nm (Figure S1e,f and Table S1).[39,48] This indicates the deprotonation of phenol−OH groups in both steps (pK_5 = 9.81(1) and pK_6 = 10.88(1)). The equilibria involving the species H_4L^{3+}, H_3L^{2+}, and H_2L show much smaller spectroscopic differences than those for the previously mentioned processes (Figures S1c,d and S2). These species present molar absorptivities doubled versus the neutral HL_{ox} species (Table S1), which accounts for the loss of the protons from the secondary amine nitrogen atoms on the backbone (pK_3 = 6.06(2) and pK_4 = 8.39(1)).

Determination of the complex formation constant of $[Ga(hox)]^{+}$ by direct pH-potentiometric method was not possible due to both the insufficient solubility of the Ga−H_2hox mixtures and the great stability of the metal complex; UV spectrophotometry was applied to individual samples following the spectral changes on the ligand absorption bands in the pH range from 0.19 to 11 (Figure S1). Samples containing the complex and different amounts of standardized HCl or NaOH were prepared, and because of the high stability of the complex even at very acidic pH, the samples were prepared and measured after 24 h, when equilibrium was achieved (see acid-assisted dissociation study in Supporting Information, Figure S4). The spectra of the Ga-hox complex collected from pH 0.19 to pH 0.95 showed identical features to those of the free ligand at the same pH values (Figure S3) suggesting the presence of the H_6L^{4+} and H_5L^{3+} species that deprotonate to the H_4L^{2+} species (λ_{max} = 245 nm and λ_{max} = 308 nm) with two well-defined isosbestic points at λ = 249 nm and λ = 346 nm, respectively (Figures S1a,b and S3a,b). There is no complex formation evidence until pH > 1, when a new band appears at λ = 368 nm as well as two isosbestic points at λ = 251 and 335 nm and the shift of the band of the free ligand at λ = 243 nm to lower energies at 260 nm due to the complex formation (Figure 3c,d). There is no further transformation along the pH range from 2 to 10.5. These data, together with the molar absorption coefficients of the different absorbing species of the free ligand (Figure S2), allowed the determination of the stability constant of the Ga-hox complex using the HypSpec program[47] (Table 3).

Table 3. Formation Constants of Ga^{3+} Complexes and pM[a] Values

log K	log K_{ML}	pGa
H_2hox[b]	34.35(1)	28.3
H_2dedpa[c]	28.11(8)	27.4
oxine (KP46)[d]	13.13(8)	
	*36.41(1)	21
NOTA[e]	30.98	27.9
DOTA[f,g]	21.33;[f] 26.05[g]	18.5; 19.50
TRAP[h]	26.24	23.1
HBED[i,j]	37.73;[i] 39.57[j]	27.7;[i] 29.4
DFO[k]	28.65	21.2

[a]Calculated at specific conditions ($[Ga^{3+}]$ = 1 μM, $[L^{x-}]$ = 10 μM, pH 7.4 and 25 °C). [b]This work (0.16 M NaCl at 25 °C). [c]From ref 27 (0.16 M NaCl at 25 °C). [d]From ref 39 (*) log K $Ga(L_{ox})_3$ (0.20 M KCl at 25 °C). [e]From ref 49 (0.10 M KCl at 25 °C). [f]From ref 50 (0.1 M KCl at 25 °C). [g]From ref 9 (0.1 M $(NMe_4)Cl$ at 25 °C). [h]From ref 18. [i]From ref 25. [j]From ref 51. [k]From ref 52.

In Figure 3b is shown the speciation plot of the Ga-hox system calculated from the stability constants from Table 3. The absorption band with maxima at 368 nm and ε = 4468 M^{-1} cm^{-1} in the $[Ga(hox)]^{+}$ complex presents similarities with that reported by Enyedy[39] for the $Ga(L_{ox})_3$ species in water at I = 0.20 M KCl and 25 °C. The molar absorptivity $Ga(L_{ox})_3$ (ε = 6627 M^{-1} cm^{-1}, calculated from their spectra) is 1.5 times the obtained value for $[Ga(hox)]^{+}$, which agrees with our results considering that, in H_2hox, there are two hydroxyquinoline chromophores.

The high log K_{ML} = 34.35(1) value of the $[Ga(hox)]^{+}$ ion characterizes H_2hox as a very high stability chelator indeed for Ga^{3+}. Even more interesting are the conditional stability constants or pM values (defined as $-\log[M_{free}]$ at [L] = 10 μM and [M] = 1 μM at pH = 7.4), which predict the stability of the complexes in vivo and allow for the most suitable

DOI: 10.1021/acs.inorgchem.8b01208
Inorg. Chem. XXXX, XXX, XXX−XXX

comparison of the relative ability of different ligands with different basicities to sequester a specific metal ion.[53,54] In Table 3 are summarized the stability constants and calculated pM values for some of the most important ^{68}Ga chelators. The Ga-hox pM value of 28.3, among the current reported ^{68}Ga chelator pM values, falls between the two literature-reported values for HBED ligand, which has an even higher pM value for Ga^{3+}. This fact, together with the presence in solution of a single species ($[Ga(hox)]^+$) in the pH range of 1−11 and considering that chelators such as DOTA, TRAP, the antitumor $Ga(L_{ox})_3$ (KP46),[39] or NOTA[55] start to hydrolyze in the pH range of 7−9, represents a distinct advantage for H_2hox and strongly suggests H_2hox as a promising ligand for gallium radiopharmaceutical compounds in a toolkit application.

^{68}Ga Labeling Experiments. Encouraged by these most promising solution studies, ^{68}Ga labeling studies were performed to investigate the coordination kinetics and radiolabeling efficiency, crucial properties for an ideal PET radiopharmaceutical based on ^{68}Ga. These studies show that H_2hox coordinates ^{68}Ga quantitatively within 5 min at room temperature (faster than do H_2dedpa, NOTA, and DOTA). DOTA, however, requires a high temperature (≥90 °C) for quantitative yields and is thus incompatible with the labeling of thermally sensitive biomolecules.[56] In our experiments, quantitative conversion (99% purity) was achieved with ligand concentrations as low as 1×10^{-7} M (Figure 4), and the molar

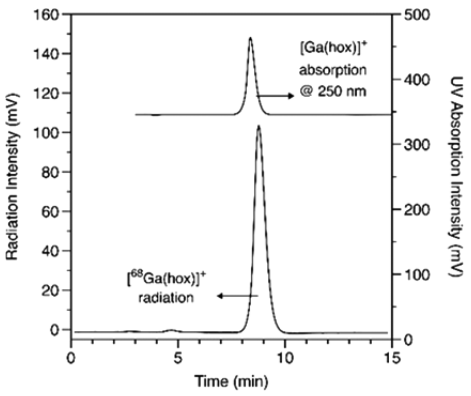

Figure 4. HPLC traces of radiation and UV absorption of the mixtures of $[^{68}Ga(hox)]^+$ ($C_L = 1 \times 10^{-7}$ M) and $[Ga(hox)]^+$ nonradioactive complex ($[Ga(hox)]^+ = 5 \times 10^{-5}$ M).

activity obtained was as high as 11 ± 1 mCi/nmol (407 ± 3.7 MBq/nmol) without any purification. The molar activity for H_2hox is even higher than that of H_2dedpa (9.8 ± 1 mCi/nmol), which was reported to be the highest obtained of all ^{68}Ga chelators with neither heating nor purification.[12,27,57] The log $D_{7.4}$ measurements showed $[^{68}Ga(hox)]^+$ was still a reasonably hydrophilic complex, with an average log $D_{7.4}$ of −0.47 ± 0.01 ($n = 4$), even though it was more lipophilic than NOTA, DOTA, and H_2dedpa.

All of these chemistry advantages characterize H_2hox as a superbly promising ligand for one-step kit-based labeling and led to in vitro and in vivo experiments. Knowing that a suitably substituted ethylenediamine precursor is available[27,35] to form an easily functionalizable $(hox)^{2-}$ ligand gave even stronger impetus to these studies.

Mouse Plasma Competition Experiments. To investigate the in vitro stability of the ^{68}Ga-hox system, a mouse plasma competition experiment was performed. $[^{68}Ga(hox)]^+$ was incubated with mouse plasma for 5, 15, 30, and 60 min at 37 °C and analyzed by radio high-performance liquid chromatography (HPLC). As shown in (Table 4), the complex was completely intact (99+%) at all time points, confirming its excellent in vitro stability of a whole half-life.

Table 4. Mouse Plasma Stability of ^{68}Ga-hox

	5 min	15 min	30 min	1 h
^{68}Ga-hox	>99%	>99%	>99%	>99%

Dynamic PET/CT Imaging. The high in vitro stability, together with the high thermodynamic stability shown by $[Ga(hox)]^+$, suggests high in vivo stability. A dynamic PET/CT imaging study in mice was therefore used to investigate the in vivo stability and biodistribution of the $[^{68}Ga(hox)]^+$ cation. As shown in Figure 5, dynamic PET/computed tomography

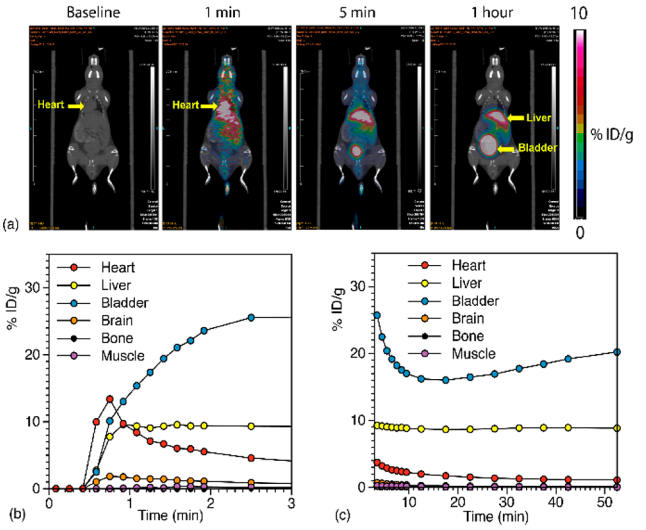

Figure 5. (a) PET/CT dynamic imaging and (b) biodistribution of $[^{68}Ga(hox)]^+$ in male (NRG) mice during (b) 0−3 min and (c) 3−53 min.

(CT) imaging showed no leakage of free ^{68}Ga, which would accumulate significantly in bone.[58] There is no accumulation in muscle as well. The complex showed quick heart uptake in the first 2 min followed by fast clearance via both hepatobiliary (liver, then gut) and renal (kidney, then bladder) pathways, which could be explained by its small size and log $D_{7.4}$ value (−0.47 ± 0.01). Even though the "naked" $[Ga(hox)]^+$ is still a hydrophilic complex based on its negative log D value, the increased lipophilicity compared with most of the high polar multiarmed carboxylate-based chelators, such as NOTA and DOTA, may elicit higher liver uptake.[29] However, recent studies with PSMA showed that the increased lipophilicity of the ^{68}Ga-PSMA tracer using a more lipophilic HBED-CC chelator translated into reduced unspecific binding and increased specific tumor cell uptake and imaging quality dramatically, compared with the conjugate using the hydrophilic DOTA chelator.[23,59] In research reported recently, Yoo and co-workers conjugated five different chelators with the same RGD peptide and investigated the effect of lipophilicity of the chelators on the biological behavior of the bioconjugates.[60] Their research also revealed that bioconju-

DOI: 10.1021/acs.inorgchem.8b01208
Inorg. Chem. XXXX, XXX, XXX−XXX

gates with more lipophilic chelators have higher tumor uptake as well as tumor/organ ratios, even though the liver uptake was increased versus those bioconjugates with polar hydrophilic chelators. Another pertinent example comes from our own work, ^{111}In-octapa-trastuzumab using a more lipophilic picolinate-based chelator showed a markedly higher tumor uptake than did ^{111}In-DOTA-trastuzumab, which suggests that, even for large biovectors, the effect of chelating moieties on the pharmacokinetic properties may not be negligible.[61] Therefore, we posit that H_2hox is a good complementary choice for the currently used chelator library in tuning the pharmacokinetics of the bioconjugates, especially for the small highly polar targeting vectors like the Glu-urea-Lys PSMA inhibitors.

The quick initial heart uptake also suggests that H_2hox could be a useful scaffold in designing lipophilic cations for heart imaging. The log *P* values between 0.8 and 1.2 have been hypothesized to be optimal for good heart imaging contrast tracers;[62,63] however, all the chelators currently used are too hydrophilic for that application. We tried to design a series of lipophilic cations based on H_2dedpa scaffold, but it is hard to increase the log *P* value to the targeted region, without increasing the molecular size too much.[34,38] Radiotracers with appropriate log *P* have also been reported using a Schiff base ligand; however, complex stability was sacrificed, because the Schiff base complex was not metabolically stable.[64−67] Therefore, we think, with this novel lipophilic H_2hox scaffold, a simple modification on the aromatic ring will increase the lipophilicity and log *P* value and would provide novel ^{68}Ga-based candidates for heart-imaging applications.

[Ga(hox)]$^+$ Fluorescence and Cell-Imaging Studies. H_2hox shows chelation-enhanced fluorescence properties. As shown in Figure 6, the peak emission wavelength of H_2hox in phosphate-buffered saline (PBS) buffer (pH = 7.4) was ∼460 nm and shifted to 560 nm once complexed with Ga^{3+}, with a fourfold increase in intensity. This property of H_2hox could encompass two major advantages over the other reported chelators. First, it could significantly inform nonradioactive metal ion complexation by monitoring fluorescence changes and concomitant dissociation of metal ion in stability studies of bifunctional chelators and could therefore provide useful information without the need of radioisotope experiments. Second, the intrinsic fluorescence could enable a bimodal tracer and direct fluorescence imaging of labeled bioconjugates without an extraneous fluorescence tag that could alter biological behavior by mutual disturbance of the two moieties and/or affect the pharmacokinetics of the radiopharmaceutical. One important advantage of a bimodal agent is that it can combine complementary information obtained from separate experiments to obtain a comprehensive synergistic analysis. For example, in a study of somatostatin receptor imaging agent, the unexpected results from in vivo PET/single photon emission computed tomography (SPECT) imaging was finally explained by optical fluorescence cellular imaging study of endocytotic uptake, benefiting from its high spatial resolution, which cannot obtained by just PET/SPECT imaging.[68] For clinical use, fluorescence techniques could also be useful through endoscopy or improve the surgical excision in fluorescence directed surgery.[69] Most of the previously reported bimodal (optical imaging and PET/SPECT) agents require one fluorophore and one radioactive moiety.[70−75] The extraneous fluorescence tag, however, may affect the metal sequestering capacity of the chelate moiety[74] or require an extra spot for bioconjugation on the biovectors[70,75] and may change the pharmacokinetics of the whole tracer as well. Therefore, H_2hox is a significant discovery to obviate this dual-modality-dual-probe problem.

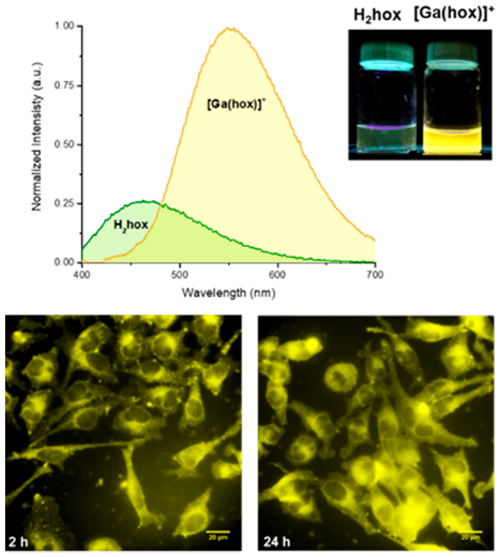

Figure 6. (upper) Fluorescence spectra of H_2hox and its Ga^{3+} complex in PBS (λ_{exc} = 365 nm, [H_2hox] = [Ga(hox)]$^+$ = 1.7 × 10^{-5} M). (lower) Time-dependent fluorescence microscopy images from HeLa cells treated with 150 μM [Ga(hox)] [ClO_4]. The scale is 20 μm.

To prove this concept, we investigated the subcellular distribution and stability of [Ga(hox)]$^+$ in living HeLa cells using fluorescence microscopy. HeLa cells were incubated with 150 μM [Ga(hox)][ClO_4] for 2 or 24 h. Bright-field images of treated cells (Figure S13) taken prior to fluorescence imaging verified the cells as viable. The morphology of HeLa cells appeared normal and suggested a low cellular toxicity of [Ga(hox)][ClO_4]. The fluorescence imaging was taken with a 520 nm emission filter, which allowed the detection of fluorescence at wavelengths greater than 520 nm (Figure 6). The complex was found to accumulate in cytoplasm, as Enyedy et al.[39] noted for the anticancer $Ga(L_{ox})_3$ complex. No obvious decomposition of the [Ga(hox)][ClO_4] complex was observed within the 24 h cellular environment, as the fluorescence intensity was constant, and the free ligand would otherwise exhibit markedly lower fluorescence intensity at wavelengths above 520 nm (Figure 6).

This proof-of-concept study showed that this chelation-enhanced fluorescence property could be used directly in intracellular distribution and stability studies, which has never been reported before with any other ligand. The intracellular distribution could provide important preparatory information for many other studies; for instance, Auger electron-based therapy requires localization of the radionuclides in the nucleus or hypoxia imaging tracers, which could be also evaluated using fluorescent imaging with a multicellular spheroid tumor model before radioactive in vivo study.[74]

CONCLUSIONS

In summary, H_2hox, as a next-generation dual-channel acyclic chelating ligand for Ga^{3+} complexation, displays an unprecedented array of properties, surpassing any ligand currently used. The synthesis of H_2hox is easier and more straightforward than that for any previously reported analogous chelator.

DOI: 10.1021/acs.inorgchem.8b01208
Inorg. Chem. XXXX, XXX, XXX−XXX

The higher thermodynamic stability of the $[Ga(hox)]^+$ complex (log K_{ML} = 34.4) compared to that of most relevant Ga^{3+} chelators and, most importantly, the largest pM value of 28.3 among those ligands proves the affinity of H_2hox toward Ga^{3+}. Moreover, H_2hox showed fast and quantitative ^{68}Ga radiolabeling at room temperature and low concentration (1×10^{-7} M) yielding a remarkably high molar activity of 11 ± 1 mCi/nmol (407 ± 3.7 MBq/nmol) without any purification. Most importantly, mouse serum stability experiments and dynamic PET imaging studies have shown high in vitro and in vivo stabilities that correlate with the high thermodynamic stability found in the solution studies. $[^{68}Ga(hox)]^+$ is also quickly cleared from the mouse via hepatobiliary and renal pathways. The lipophilicity of H_2hox provides a choice complementary to the current library of chelators, to tune the pharmacokinetics of bioconjugates and design lipophilic tracers for heart imaging or cell labeling. The intrinsic fluorescence of $[Ga(hox)]^+$ imaged HeLa cancer cells showing accumulation in the cytoplasm and suggests strongly that this compound could serve in dual-channel (bimodal) imaging or fluorescence-directed surgery. The fluorescence emission red shift and intensity increase (chelation-enhanced fluorescence) upon the complexation of H_2hox with Ga^{3+} could be directly used to study the stability of a nonradioactive bioconjugate in vitro. The high affinity of H_2hox for Ga^{3+}, confirmed in solution as well as in vitro and in vivo, together with the fast quantitative radiolabeling at low concentrations and mild conditions encourage the use of H_2hox for development of a convenient toolkit radiopharmaceutical compound. Current efforts are focused on bifunctional analogues of the H_2hox scaffold.

EXPERIMENTAL SECTION

Materials and Methods. All solvents and reagents were purchased from commercial sources (TCI America, Sigma-Aldrich, Fisher Scientific) and used as received unless otherwise indicated. The analytical thin-layer chromatography (TLC) plates used were aluminum-backed ultrapure silica gel 60 Å, 250 μm thickness; ^1H and ^{13}C NMR spectra were recorded at ambient temperature on Bruker Avance 300 and Avance 400 spectrometers; the ^1H NMR spectra were calibrated against residual protio-solvent peak, and the ^{13}C NMR spectra were referenced to the deuterated solvent. Low-resolution mass spectrometry was performed on a Waters ZG spectrometer with an electrospray/chemical-ionization (ESCI) source, and high-resolution electrospray ionization mass spectrometry (ESI-MS) was performed on a Micromass LCT time-of-flight (TOF) instrument. Microanalyses for C, H, and N were performed on a Carlo Erba Elemental Analyzer EA 1108. Purification and quality control of $[^{68}Ga(hox)]^+$ were performed on an Agilent HPLC system equipped with a model 1200 quaternary pump, a model 1200 UV absorbance detector, and a Bioscan NaI scintillation detector. The radiodetector was connected to a Bioscan B-FC-1000 Flow-count system, and the output from the Bioscan Flow-count system was fed into an Agilent 35900E Interface, which converted the analog signal to digital. The operation of the Agilent HPLC system was controlled using the Agilent ChemStation software. The HPLC columns used were a semipreparative column (Phenomenex C18, 5 μ, 250 × 10 mm) and an analytical column (Phenomenex C18, 5 μ, 250 × 4.6 mm). The HPLC solvents were A: H_2O containing 0.1% trifluoroacetic acid (TFA) and B: CH_3CN containing 0.1% TFA. PET imaging experiments were conducted using a Siemens Inveon microPET/CT scanner.

Synthesis and Characterization. 8-Hydroxyquinoline-2-carboxaldehyde (**1**). A mixture of 8-hydroxyl-2-methylquinoline (31 mmol, 5 g) and selenium dioxide (35 mmol, 3.9 g) was stirred in 250 mL of 1,4-diethylene at 80 °C overnight. Diatomaceous earth (5 g) was added after the mixture cooled, and the mixture was filtered. The filtrate was evaporated to solid crude and was purified by silica-gel column chromatography (hexane/ethyl acetate, 10:90 to 50:50, v/v) to obtain pure yellow needle crystal product (25 mmol, 4.4 g). Yield = 82%. ^1H NMR (300 MHz, $CDCl_3$) δ 10.21 (d, J = 0.9 Hz, 1H), 8.32 (dd, J = 8.5, 0.8 Hz, 1H), 8.15 (s, 1H), 8.05 (d, J = 8.5 Hz, 1H), 7.62 (t, J = 8.0 Hz, 1H), 7.42 (dd, J = 8.3, 1.2 Hz, 1H), 7.28 (dd, J = 7.7, 1.3 Hz, 1H). ^{13}C NMR (75 MHz, $CDCl_3$) δ 192.8, 153.1, 150.3, 138.0, 137.6, 131.1, 130.6, 118.2, 118.1, 111.4, 77.2.

H_2hox (**2**). 8-Hydroxyquinoline-2-carboxaldehyde (**1**) (11.6 mmol, 2 g) was dissolved in 50 mL of ethanol; ethylenediamine (5.8 mmol, 387 μL) dissolved in 5 mL of ethanol was added dropwise, and the reaction mixture was stirred at 60 °C for 4 h. A light yellow precipitation formed and was collected and resuspended in 50 mL of ethanol. $NaBH_4$ (5 equiv) was added in portions, and the reaction mixture was stirred at room temperature overnight. HCl (20 mL; 6 M) was added then and stirred for 4 h to quench the reaction. The pH of the reaction mixture was then readjusted to neutral using NaOH (2 M), and the white precipitation was filtered and dried as crude product. The crude product was further washed with water and methanol to obtain the pure product (5.2 mmol, 1.97 g). Yield = 87%. ^1H NMR (300 MHz, MeOD) δ 8.21 (d, J = 8.5 Hz, 1H), 7.50−7.38 (m, 2H), 7.36 (dd, J = 8.3, 1.6 Hz, 1H), 7.10 (dd, J = 7.3, 1.6 Hz, 1H), 4.20 (s, 2H), 3.03 (s, 2H). ^{13}C NMR (75 MHz, MeOD) δ 157.4, 154.1, 139.2, 138.1, 129.5, 128.4, 122.0, 119.0, 112.3, 54.7, 49.0, 48.8. LSMS m/z = 375.2. The product was recrystallized using methanol to obtain colorless needle crystals. H_2hox 2HCl used for titration was synthesized by mixing a solution of H_2hox (**3**) in tetrahydrofuran (THF) and 6 M HCl and drying in vacuo to afford a white powder. LR-ESI-MS calcd for $C_{22}H_{23}N_4O_2$: m/z = 375.2; found: 375.2 $[M + H]^+$. H_2hox·2HCl used for titration was synthesized by mixing a solution of H_2hox (**2**) in THF and 6 M HCl and drying in vacuo to afford a white powder. Elemental analysis: H_2hox·2HCl·0.5 H_2O, calcd % for C 57.9, H 5.52, N 12.28; found: C 58.24, H 5.30, N 11.90.

$[Ga(hox)][ClO_4]$(**4**). H_2hox (40 mg, 0.107 mmol) was dissolved in acetonitrile. $Ga(ClO_4)_3·6H_2O$ (55 mg, 0.116 mmol) was added, and the pH was adjusted to ∼5 using 0.1 M NaOH. The reaction mixture was stirred for 1 h at 50 °C, dichloromethane (DCM) was added to extract the product, and a yellow crystal suitable for X-ray diffraction formed from layer diffusion of diethyl ether into the DCM extraction layer.^1H NMR (300 MHz, MeOD) δ 8.81 (d, J = 8.5 Hz, 1H), 7.87 (d, J = 8.5 Hz, 1H), 7.76−7.53 (m, 1H), 7.41 (d, J = 8.3 Hz, 1H), 7.00 (d, J = 7.7 Hz, 1H), 4.76 (d, J = 17.8 Hz, 1H), 4.38 (d, J = 17.9 Hz, 1H), 3.11 (d, J = 10.0 Hz, 1H), 2.63 (d, J = 9.9 Hz, 1H). ^{13}C NMR (75 MHz, MeOD) δ 155.9, 150.2, 142.7, 134.9, 131.2, 128.6, 120.2, 113.1, 112.7, 49.7. LR-ESI-MS for M^+ of $C_{22}H_{22}{}^{69}GaN_4O_2$: calcd m/z = 441.1; found 441.0. Elemental analysis for $[Ga(hox)][ClO_4]·H_2O$, calcd % C 47.22, H 3.96, N 10.01; found C47.19, H 3.84, N 9.72.

X-ray Crystallography. Colorless tablet-shaped crystals of H_2hox were obtained by recrystallization from methanol. X-ray diffraction data of a suitable crystal were collected using a Bruker APEX II area detector diffractometer with Mo Kα radiation. The structure was solved in the monoclinic $P2_1/c$ space group. Yellow blade crystals of $[Ga(hox)][ClO_4]$ suitable for X-ray diffraction were obtained layer diffusion of diethyl ether into the DCM solution of the complex. X-ray diffraction data of a suitable crystal was collected on a Bruker APEX DUO diffractometer using Mo Kα radiation. The structure was solved in the monoclinic $C2/c$ space group. All non-hydrogen atoms were refined anisotropically. All N−H hydrogen atoms were located in difference maps and refined isotropically. All other hydrogen atoms were placed in calculated positions. Further structural refinement details and the .cif files are available in the Supporting Information.

DFT and TDDFT Calculations. All calculations were performed using the Gaussian 09 package (Revision D.01). Full geometry optimizations of the $[Ga(hox)]^+$ were performed with the CAM-B3LYP hybrid exchange−correlation functional[76] in aqueous solution using the polarizable continuum model (PCE).[77] Geometry optimizations were performed using the 6-311+G(d,p) basis set on

DOI: 10.1021/acs.inorgchem.8b01208
Inorg. Chem. XXXX, XXX, XXX−XXX

first- and second-row elements and the Los Alamos effect core potential (ECP) and valence basis set of double-ζ quality (LANL2DZ) on the Ga atom.[78] The input coordinate of atoms was adapted from the crystal structure of the [Ga(hox)][ClO_4] complex, and no constraints on symmetry were imposed during the geometry optimization. The resulting geometries showed no imaginary frequencies and thus were confirmed to be minima on the potential energy surfaces. The PBE0 hybrid functional[79] and the same basis set and ECP was employed to simulate the UV−vis absorption features of the fully optimized structure and generate its ground-state molecular electrostatic potential (MEP) mapping.

Solution Thermodynamics. Protonation constants and metal stability constants were calculated from UV spectrophotometric titration data obtained using a Cary60 UV−vis spectrophotometer in the spectral range of 200−450 nm. The path length was 1 cm for all the samples. Individual samples of 5 mL containing the ligand (H_2hox, 2.72×10^{-5} M) or the corresponding gallium complex ($[Ga(hox)]^+$, 2.82×10^{-5} M) in pure water were prepared by adjusting the pH with different amounts of standardized HCl or NaOH solutions, and NaCl was added to maintain a constant 0.16 M ionic strength between the pH range of 0.8−11.85. A Ross combination pH electrode was daily calibrated for hydrogen ion concentrations using HCl as described before,[37] and the results were analyzed by the Gran[80] procedure. pH was measured in ligand and metal−ligand samples between the pH range of 2.0−11.5.

In the samples below pH 0.8, it was not possible to maintain constant the ionic strength, since that depends on the HCl content, and the equilibrium H^+ concentration was calculated from solution stoichiometry, not measured with a glass electrode. For the solutions of high acidity, the correct acidity scale H^0 was used.[81] For the ligand protonation equilibria study up to 2 min was attained at 25 °C to reach the equilibrium before measuring the pH and the UV absorption spectrum. For the samples containing the metal−ligand complex, the measurements were performed only after 24 h when the equilibrium had been achieved. The protonation constants of H_2hox and the Ga(III) complex stability constants were calculated from the experimental data using the HypSpec2014[47] program. Proton dissociation constants corresponding to hydrolysis of Ga(III) aqueous ions included in the calculations were taken from Baes and Mesmer.[82] The species formed in the studied systems are characterized by the general equilibrium: $pM + qH + rL = M_pH_qL_r$ (charges omitted). For convention, a complex containing a metal ion M, proton H, and ligand L has the general formula $M_pH_qL_r$. The stoichiometric indices p might also be 0 in the case of protonation equilibria, and negative values of q refer to proton removal or hydroxide ion addition during formation of the complex. The overall equilibrium constant for the formation of the complexes $M_pH_qL_r$ from its components is designated as log β. Stepwise equilibrium constants log K correspond to the difference in log units between the overall constants of sequentially protonated (or hydroxide) species. pM is defined as $(-\log[M^{n+}]_{free})$ and is calculated at specific conditions ($[M^{n+}] = 1$ μM, $[L^{x-}] = 10$ μM, pH 7.4 and 25 °C.

The acid-assisted dissociation kinetic study of the Ga(III)-hox complex was performed by measuring the UV spectra in the same experimental conditions as described above. Concentrated standardized HCl was added to a Ga-hox stock solution ($[Ga(hox)]^+ = 2.82 \times 10^{-5}$ M) to achieve pH 1. The reaction was followed by registering the spectra at 15 min intervals at 25 °C.

$[^{68}Ga(hox)]^+$ Labeling Procedure. ^{68}Ga was obtained from an Eckert & Ziegler IGG100 ^{68}Ga generator and was purified according to the previously published procedures[83] using DGA resin column. Radioactivity of $[^{68}Ga(hox)]^+$ was measured using a Capintec CRC −25R/W dose calibrator. $[^{68}Ga(hox)]^+$ was also obtained by adding 0.2 mCi purified ^{68}Ga to 200 mL of a 1×10^{-7} M solution of H_2hox in 0.1 M NaOAc solution (pH 8.5) and left for 5 min at RT. The reaction progress was monitored by analytical HPLC eluted with 84/16 phosphate buffer (pH 7.4)/CH_3CN at a flow rate of 2 mL/min. The retention time of $[^{68}Ga(hox)]^+$ was 8.6 min.

Log $D_{7.4}$ Measurements. Aliquots (2 μL) of the $[^{68}Ga(hox)]^+$ were added to a vial containing 3 mL of octanol and 3 mL of 0.1 M phosphate buffer (pH 7.4). The mixture was vortexed for 1 min and then centrifuged for 10 min. Samples of the octanol (1 mL) and buffer (1 mL) layers were taken and counted. The log $D_{7.4}$ value was calculated using eq 1.

$$\log D_{7.4} = \log_{10}\left(\frac{\text{counts in octanol phase}}{\text{counts in buffer phase}}\right) \quad (1)$$

Stability in Mouse Plasma. Purified ^{68}Ga in 0.5 mL of water was added into a 4 mL glass vial preloaded with 0.7 mL of 4-(2-hydroxyethyl)-1-piperazineethanesulfonic acid (HEPES) buffer (2 M, pH 5.0) and 25 nmol of H_2hox. The radiolabeling reaction was performed under microwave heating for 1 min. The reaction mixture was purified by HPLC using the semipreparative column eluted with 83/17 A/B (A: H_2O containing 0.1% TFA, and B: CH_3CN containing 0.1% TFA) at a flow rate of 4.5 mL/min. The retention time of $[^{68}Ga(hox)]^+$ was 13.8 min. The eluate fraction containing the radiolabeled product was collected, diluted with water (50 mL), and passed through a C18 Sep-Pak cartridge that was prewashed with ethanol (10 mL) and water (10 mL). After the C18 Sep-Pak cartridge was washed with water (10 mL), the ^{68}Ga-labeled product was eluted off the cartridge with ethanol (0.4 mL), dried by helium, and redissolved with saline (0.5 mL) for plasma stability and imaging studies. Aliquots (20 μL) of the $[^{68}Ga(hox)]^+$ were incubated with 80 μL of mouse plasma for 5, 15, 30, and 60 min at 37 °C. At the end of each incubation period, samples were quenched with 100 μL of 70% CH_3CN and centrifuged for 20 min. The metabolites were measured using a semipreparative HPLC system with the same HPLC conditions as described for the purification of $[^{68}Ga(hox)]^+$.

PET/CT Imaging Studies. PET/CT imaging studies were conducted in accordance with the guidelines established by the Canadian Council on Animal Care and approved by the Animal Ethics Committee of the University of British Columbia. Male NOD.Cg-Rag1^{tm1Mom} Il2rg^{tm1Wjl}/SzJ (NRG) mice were purchased from in-house colonies at the Animal Research Centre, BC Cancer Research Centre, Vancouver, Canada. PET/CT imaging experiments were conducted using a Siemens Inveon microPET/CT scanner. Mice were sedated with 2% isoflurane in oxygen inhalation and positioned in the scanner. A baseline CT scan was obtained for localization and attenuation correction before radiotracer injection, using 80 kV X-rays at 500 mA, three sequential bed positions with 34% overlap, and 180° continuous rotation. The mice were kept warm by a heating pad during acquisition. The dynamic acquisition of 60 min was started at the time of intravenous injection with ∼3.4−4.0 MBq of ^{68}Ga−H_2hox. The list mode data were rebinned into time intervals (12 × 10, 8 × 60, 7 × 300, 1 × 900 s) to obtain tissue time−activity curves. Images were reconstructed using iterative three-dimensional ordered subset expectation maximization (OSEM3D, two iterations) using maximum a priori with shifted poisson distribution (SP-MAP, 18 iterations).

Fluorescence Microscopy. Hela cells were purchased from the American Type Culture Collection (ATCC). Cells were grown in Eagle's Minimal Essential Medium (MEM) supplemented with heat-inactivated 10% fetal bovine serum, 1 mM sodium pyruvate, 4 mM L-glutamine, and 1% nonessential amino acids in a humidified incubator at 37 °C and 5% CO_2. Cells were seeded eight-well culture slips 24 h prior to treatment. The [Ga(hox)][ClO_4] working solution for fluorescence microscopy was prepared from a PBS stock solution. No precipitation of the compound was observed in the working solution under this condition. Cells were exposed to 150 uM [Ga(hox)]-[ClO_4] for 2 and 24 h and washed with PBS, and imaging was done using a fluorescence microscope BX40, a U-MWU filter cube, an F-View CCD camera (all Olympus), Cell-F fluorescence imaging software (Olympus), and a 60× magnification oil immersion objective lens.

DOI: 10.1021/acs.inorgchem.8b01208
Inorg. Chem. XXXX, XXX, XXX−XXX

■ ASSOCIATED CONTENT

Supporting Information

The Supporting Information is available free of charge on the ACS Publications website at DOI: 10.1021/acs.inorgchem.8b01208.

Detailed information on ^{1}H NMR and ^{13}C NMR spectra of compounds, spectrophotometric measurements, X-ray crystallography data (including tables of bond lengths and angles), DFT-optimized geometries and bond parameters, detailed HPLC radio-traces, and detailed data of all biodistribution studies (PDF)

Accession Codes

CCDC 1811769−1811770 contain the supplementary crystallographic data for this paper. These data can be obtained free of charge via www.ccdc.cam.ac.uk/data_request/cif, or by emailing data_request@ccdc.cam.ac.uk, or by contacting The Cambridge Crystallographic Data Centre, 12 Union Road, Cambridge CB2 1EZ, UK; fax: +44 1223 336033.

■ AUTHOR INFORMATION

Corresponding Author

*E-mail: orvig@chem.ubc.ca.

ORCID

Yang Cao: 0000-0001-8636-7919

Kuo-Shyan Lin: 0000-0002-0739-0780

Chris Orvig: 0000-0002-2830-5493

Funding

Funding for this work was provided to C.O. by the Natural Sciences and Engineering Research Council (NSERC) of Canada as a Discovery Grant (RGPIN-42394-13), as well as by NSERC (CHRP 493725-16) and the Canadian Institutes of Health Research (CIHR, CPG-146482) as a Collaborative Health Research Project.

Notes

The authors declare no competing financial interest.

■ ACKNOWLEDGMENTS

M. V. Tran, J. Chen, and J. Cudmore are thanked for their important assistance.

■ REFERENCES

(1) Green, M. A. The potential for generator-based PET perfusion tracers. *J. Nucl. Med.* **1990**, *31*, 1641.

(2) Blower, P. J. A nuclear chocolate box: the periodic table of nuclear medicine. *Dalton Trans.* **2015**, *44*, 4819.

(3) Baranyai, Z.; Reich, D.; Vagner, A.; Weineisen, M.; Toth, I.; Wester, H. J.; Notni, J. A shortcut to high-affinity Ga-68 and Cu-64 radiopharmaceuticals: one-pot click chemistry trimerisation on the TRAP platform. *Dalton Trans.* **2015**, *44*, 11137.

(4) Ferreira, C. L.; Lamsa, E.; Woods, M.; Duan, Y.; Fernando, P.; Bensimon, C.; Kordos, M.; Guenther, K.; Jurek, P.; Kiefer, G. E. Evaluation of bifunctional chelates for the development of gallium-based radiopharmaceuticals. *Bioconjugate Chem.* **2010**, *21*, 531.

(5) Notni, J.; Reich, D.; Maltsev, O. V.; Kapp, T. G.; Steiger, K.; Hoffmann, F.; Esposito, I.; Weichert, W.; Kessler, H.; Wester, H.-J. In Vivo PET Imaging of the Cancer Integrin $\alpha v\beta 6$ Using 68Ga-Labeled Cyclic RGD Nonapeptides. *J. Nucl. Med.* **2017**, *58*, 671.

(6) Young, J. D.; Abbate, V.; Imberti, C.; Meszaros, L. K.; Ma, M. T.; Terry, S. Y. A.; Hider, R. C.; Mullen, G. E.; Blower, P. J. (68)Ga-THP-PSMA: A PET Imaging Agent for Prostate Cancer Offering Rapid, Room-Temperature, 1-Step Kit-Based Radiolabeling. *J. Nucl. Med.* **2017**, *58*, 1270.

(7) Tsionou, M. I.; Knapp, C. E.; Foley, C. A.; Munteanu, C. R.; Cakebread, A.; Imberti, C.; Eykyn, T. R.; Young, J. D.; Paterson, B. M.; Blower, P. J.; Ma, M. T. Comparison of macrocyclic and acyclic chelators for gallium-68 radiolabelling. *RSC Adv.* **2017**, *7*, 49586.

(8) Bianchi, A.; Calabi, L.; Giorgi, C.; Losi, P.; Mariani, P.; Paoli, P.; Rossi, P.; Valtancoli, B.; Virtuani, M. Thermodynamic and structural properties of Gd3+ complexes with functionalized macrocyclic ligands based upon 1,4,7,10-tetraazacyclododecane. *J. Chem. Soc., Dalton Trans.* **2000**, 697.

(9) Kubicek, V.; Havlickova, J.; Kotek, J.; Tircso, G.; Hermann, P.; Toth, E.; Lukes, I. Gallium(III) complexes of DOTA and DOTA-monoamide: kinetic and thermodynamic studies. *Inorg. Chem.* **2010**, *49*, 10960.

(10) Zhernosekov, K. P.; Filosofov, D. V.; Baum, R. P.; Aschoff, P.; Bihl, H.; Razbash, A. A.; Jahn, M.; Jennewein, M.; Rosch, F. Processing of generator-produced 68Ga for medical application. *J. Nucl. Med.* **2007**, *48*, 1741.

(11) Eppard, E.; Wuttke, M.; Nicodemus, P. L.; Rosch, F. Ethanol-Based Post-processing of Generator-Derived (6)(8)Ga Toward Kit-Type Preparation of (6)(8)Ga-Radiopharmaceuticals. *J. Nucl. Med.* **2014**, *55*, 1023.

(12) Velikyan, I.; Beyer, G. J.; Langstrom, B. Microwave-supported preparation of (68)Ga bioconjugates with high specific radioactivity. *Bioconjugate Chem.* **2004**, *15*, 554.

(13) Ma, M. T.; Blower, P. J. In *Metal Chelation in Medicine;* The Royal Society of Chemistry, 2017; p 260.

(14) Velikyan, I.; Maecke, H.; Langstrom, B. Convenient preparation of 68Ga-based PET-radiopharmaceuticals at room temperature. *Bioconjugate Chem.* **2008**, *19*, 569.

(15) de Sa, A.; Matias, A. A.; Prata, M. I.; Geraldes, C. F.; Ferreira, P. M.; Andre, J. P. Gallium labeled NOTA-based conjugates for peptide receptor-mediated medical imaging. *Bioorg. Med. Chem. Lett.* **2010**, *20*, 7345.

(16) Prata, M. I.; Santos, A. C.; Geraldes, C. F.; de Lima, J. J. Structural and in vivo studies of metal chelates of Ga(III) relevant to biomedical imaging. *J. Inorg. Biochem.* **2000**, *79*, 359.

(17) Simecek, J.; Schulz, M.; Notni, J.; Plutnar, J.; Kubicek, V.; Havlickova, J.; Hermann, P. Complexation of metal ions with TRAP (1,4,7-triazacyclononane phosphinic acid) ligands and 1,4,7-triazacyclononane-1,4,7-triacetic acid: phosphinate-containing ligands as unique chelators for trivalent gallium. *Inorg. Chem.* **2012**, *51*, 577.

(18) Notni, J.; Hermann, P.; Havlickova, J.; Kotek, J.; Kubicek, V.; Plutnar, J.; Loktionova, N.; Riss, P. J.; Rosch, F.; Lukes, I. A triazacyclononane-based bifunctional phosphinate ligand for the preparation of multimeric 68Ga tracers for positron emission tomography. *Chem. - Eur. J.* **2010**, *16*, 7174.

(19) Waldron, B. P.; Parker, D.; Burchardt, C.; Yufit, D. S.; Zimny, M.; Roesch, F. Structure and stability of hexadentate complexes of ligands based on AAZTA for efficient PET labelling with gallium-68. *Chem. Commun.* **2013**, *49*, 579.

(20) Nock, B. A.; Kaloudi, A.; Nagel, J.; Sinnes, J. P.; Roesch, F.; Maina, T. Novel bifunctional DATA chelator for quick access to site-directed PET (68)Ga-radiotracers: preclinical proof-of-principle with [Tyr(3)]octreotide. *Dalton Trans.* **2017**, *46*, 14584.

(21) Parker, D.; Waldron, B. P.; Yufit, D. S. Crystallographic and solution NMR structural analyses of four hexacoordinated gallium-(III) complexes based on ligands derived from 6-amino-perhydro-1,4-diazepine. *Dalton Trans.* **2013**, *42*, 8001.

(22) Ferreira, C. L.; Yapp, D. T.; Mandel, D.; Gill, R. K.; Boros, E.; Wong, M. Q.; Jurek, P.; Kiefer, G. E. (68)Ga small peptide imaging: comparison of NOTA and PCTA. *Bioconjugate Chem.* **2012**, *23*, 2239.

(23) Eder, M.; Schafer, M.; Bauder-Wust, U.; Hull, W. E.; Wangler, C.; Mier, W.; Haberkorn, U.; Eisenhut, M. 68Ga-complex lipophilicity and the targeting property of a urea-based PSMA inhibitor for PET imaging. *Bioconjugate Chem.* **2012**, *23*, 688.

(24) Afshar-Oromieh, A.; Malcher, A.; Eder, M.; Eisenhut, M.; Linhart, H. G.; Hadaschik, B. A.; Holland-Letz, T.; Giesel, F. L.; Kratochwil, C.; Haufe, S.; Haberkorn, U.; Zechmann, C. M. PET imaging with a [68Ga]gallium-labelled PSMA ligand for the diagnosis

DOI: 10.1021/acs.inorgchem.8b01208
Inorg. Chem. XXXX, XXX, XXX−XXX

of prostate cancer: biodistribution in humans and first evaluation of tumour lesions. *Eur. J. Nucl. Med. Mol. Imaging* **2013**, *40*, 486.
(25) Motekaitis, R. J.; Sun, Y.; Martell, A. E.; Welch, M. J. Stabilities of Gallium(Iii), Iron(Iii), and Indium(Iii) Chelates of Hydroxyaromatic Ligands with Different Overall Charges. *Inorg. Chem.* **1991**, *30*, 2737.
(26) Andre, J. P.; Maecke, H. R.; Zehnder, M.; Macko, L.; Akyel, K. G. 1,4,7-triazacyclononane-1-succinic acid-4,7-diacetic acid (NODA-SA): a new bifunctional chelator for radio gallium-labelling of biomolecules. *Chem. Commun.* **1998**, 1301.
(27) Boros, E.; Ferreira, C. L.; Cawthray, J. F.; Price, E. W.; Patrick, B. O.; Wester, D. W.; Adam, M. J.; Orvig, C. Acyclic chelate with ideal properties for (68)Ga PET imaging agent elaboration. *J. Am. Chem. Soc.* **2010**, *132*, 15726.
(28) Bollinger, J. E.; Mague, J. T.; O'Connor, C. J.; Banks, W. A.; Roundhill, D. M. Lipophilic Hexadentate Gallium, Indium and Iron Complexes of New Phenolate-Derivatized Cyclohexanetriamines as Potential in-Vivo Metal-Transfer Reagents. *J. Chem. Soc., Dalton Trans.* **1995**, 1677.
(29) Price, E. W.; Orvig, C. Matching chelators to radiometals for radiopharmaceuticals. *Chem. Soc. Rev.* **2014**, *43*, 260.
(30) Farkas, E.; Nagel, J.; Waldron, B. P.; Parker, D.; Toth, I.; Brucher, E.; Rosch, F.; Baranyai, Z. Equilibrium, Kinetic and Structural Properties of Gallium(III) and Some Divalent Metal Complexes Formed with the New DATA(m) and DATA(5m) Ligands. *Chem. - Eur. J.* **2017**, *23*, 10358.
(31) Baranyai, Z.; Uggeri, F.; Maiocchi, A.; Giovenzana, G. B.; Cavallotti, C.; Takacs, A.; Toth, I.; Banyai, I.; Benyei, A.; Brucher, E.; Aime, S. Equilibrium, Kinetic and Structural Studies of AAZTA Complexes with Ga3+, In3+ and Cu2+. *Eur. J. Inorg. Chem.* **2013**, *2013*, 147.
(32) Vágner, A.; D'Alessandria, C.; Gambino, G.; Schwaiger, M.; Aime, S.; Maiocchi, A.; Tóth, I.; Baranyai, Z.; Tei, L. A rigidified AAZTA-like ligand as efficient chelator for68Ga radiopharmaceuticals. *ChemistrySelect* **2016**, *1*, 163.
(33) Fellner, M.; Riss, P.; Loktionova, N.; Zhernosekov, K.; Thews, O.; Geraldes, C. F. G. C.; Kovacs, Z.; Lukes, I.; Rosch, F. Comparison of different phosphorus-containing ligands complexing Ga-68 for PET-imaging of bone metabolism. *Radiochim. Acta* **2011**, *99*, 43.
(34) Boros, E.; Ferreira, C. L.; Patrick, B. O.; Adam, M. J.; Orvig, C. New Ga derivatives of the H2dedpa scaffold with improved clearance and persistent heart uptake. *Nucl. Med. Biol.* **2011**, *38*, 1165.
(35) Boros, E.; Ferreira, C. L.; Yapp, D. T. T.; Gill, R. K.; Price, E. W.; Adam, M. J.; Orvig, C. RGD Conjugates Of The H2Dedpa scaffold: Synthesis, labelling and imaging with 68Ga. *Nucl. Med. Biol.* **2012**, *39*, 785.
(36) Ramogida, C. F.; Cawthray, J. F.; Boros, E.; Ferreira, C. L.; Patrick, B. O.; Adam, M. J.; Orvig, C. H2CHXdedpa and H4CHXoctapa - chiral acyclic chelating ligands for 67/68Ga and 111In radiopharmaceuticals. *Inorg. Chem.* **2015**, *54*, 2017.
(37) Weekes, D. M.; Ramogida, C. F.; Jaraquemada-Pelaez, M. G.; Patrick, B. O.; Apte, C.; Kostelnik, T. I.; Cawthray, J. F.; Murphy, L.; Orvig, C. Dipicolinate Complexes of Gallium(III) and Lanthanum(III). *Inorg. Chem.* **2016**, *55*, 12544.
(38) Ramogida, C. F.; Schindler, D.; Schneider, C.; Tan, Y. L. K.; Huh, S.; Ferreira, C. L.; Adam, M. J.; Orvig, C. Synthesis and characterization of lipophilic cationic Ga(III) complexes based on the H(2)CHXdedpa and H(2)dedpa ligands and their Ga-67/68 radiolabeling studies. *RSC Adv.* **2016**, *6*, 103763.
(39) Enyedy, E. A.; Domotor, O.; Varga, E.; Kiss, T.; Trondl, R.; Hartinger, C. G.; Keppler, B. K. Comparative solution equilibrium studies of anticancer gallium(III) complexes of 8-hydroxyquinoline and hydroxy(thio)pyrone ligands. *J. Inorg. Biochem.* **2012**, *117*, 189.
(40) Hata, T.; Uno, T. Studies on new derivatives of 8-quinolinol as chelating agents. I. Syntheses, coloration reaction with metal ions and acid dissociation constants of some azomethine and aminomethyl derivatives. *Bull. Chem. Soc. Jpn.* **1972**, *45*, 477.
(41) Hata, T.; Uno, T. Studies on New Derivatives of 8-Quinolinol as Chelating Agents. II. Chelate Formation of Some Aminomethyl Derivatives Derived from 8-Hydroxyquinoline-2-carbaldehyde with Metal Ions. *Bull. Chem. Soc. Jpn.* **1972**, *45*, 2497.
(42) Li, L. H.; Xu, B. Synthesis and characterization of 5-substituted 8-hydroxyquinoline derivatives and their metal complexes. *Tetrahedron* **2008**, *64*, 10986.
(43) Mishra, A.; Periasamy, N.; Patankar, M. P.; Narasimhan, K. L. Synthesis and characterisation of soluble aluminium complex dyes based on 5-substituted-8-hydroxyquinoline derivatives for OLED applications. *Dyes Pigm.* **2005**, *66*, 89.
(44) Prachayasittikul, V.; Prachayasittikul, S.; Ruchirawat, S.; Prachayasittikul, V. 8-Hydroxyquinolines: a review of their metal chelating properties and medicinal applications. *Drug Des., Dev. Ther.* **2013**, *7*, 1157.
(45) Gonzalez-Vera, J. A.; Lukovic, E.; Imperiali, B. Synthesis of red-shifted 8-hydroxyquinoline derivatives using click chemistry and their incorporation into phosphorylation chemosensors. *J. Org. Chem.* **2009**, *74*, 7309.
(46) Xie, J. T.; Ning, Z. J.; Tian, H. A soluble 5-carbazolium-8-hydroxyquinoline Al(III) complex as a dipolar luminescent material. *Tetrahedron Lett.* **2005**, *46*, 8559.
(47) Gans, P.; Sabatini, A.; Vacca, A. Determination of equilibrium constants from spectrophometric data obtained from solutions of known pH: The program pHab. *Ann. Chim-Rome* **1999**, *89*, 45.
(48) Xia, Y. X.; Chen, J. F.; Choppin, G. R. Solubility, dissociation and complexation with Nd(III) and Th(IV) of oxine, thenoyltrifluoroacetone and 1,10-phenanthroline in 5.0 m NaCl. *Talanta* **1996**, *43*, 2073.
(49) Heppeler, A.; Froidevaux, S.; Macke, H. R.; Jermann, E.; Behe, M.; Powell, P.; Hennig, M. Radiometal-labelled macrocyclic chelator-derivatised somatostatin analogue with superb tumour-targeting properties and potential for receptor-mediated internal radiotherapy. *Chem. - Eur. J.* **1999**, *5*, 1974.
(50) Clarke, E. T.; Martell, A. E. Stabilities of Trivalent Metal-Ion Complexes of the Tetraacetate Derivatives of 12-Membered, 13-Membered and 14-Membered Tetraazamacrocycles. *Inorg. Chim. Acta* **1991**, *190*, 37.
(51) Motekaitis, R. J.; Martell, A. E.; Welch, M. J. Stabilities of Trivalent Metal-Complexes of Phenolic Ligands Related to N,N′-Bis(2-Hydroxybenzyl)Ethylenediamine-N,N′-Diacetic Acid (Hbed). *Inorg. Chem.* **1990**, *29*, 1463.
(52) Evers, A.; Hancock, R. D.; Martell, A. E.; Motekaitis, R. J. Metal ion recognition in ligands with negatively charged oxygen donor groups. Complexation of iron(III), gallium(III), indium(III), aluminum(III), and other highly charged metal ions. *Inorg. Chem.* **1989**, *28*, 2189.
(53) Liu, Z. D.; Khodr, H. H.; Liu, D. Y.; Lu, S. L.; Hider, R. C. Synthesis, Physicochemical Characterization, and Biological Evaluation of 2-(1′-Hydroxyalkyl)-3-hydroxypyridin-4-ones: Novel Iron Chelators with Enhanced pFe3+Values†. *J. Med. Chem.* **1999**, *42*, 4814.
(54) Crisponi, G.; Nurchi, V. M. In *Chelation Therapy in the Treatment of Metal Intoxication;* Academic Press: Boston, MA, 2016; p 35.
(55) Clarke, E. T.; Martell, A. E. Stabilities of the Fe(III), Ga(III) and In(III) chelates of *N,N′,N″*-triazacyclononanetriacetic acid. *Inorg. Chim. Acta* **1991**, *181*, 273.
(56) Meyer, G. J.; Macke, H.; Schuhmacher, J.; Knapp, W. H.; Hofmann, M. 68Ga-labelled DOTA-derivatised peptide ligands. *Eur. J. Nucl. Med. Mol. Imaging* **2004**, *31*, 1097.
(57) Harris, W. R.; Pecoraro, V. L. Thermodynamic binding constants for gallium transferrin. *Biochemistry* **1983**, *22*, 292.
(58) Sephton, R. G.; Hodgson, G. S.; De Abrew, S.; Harris, A. W. Ga-67 and Fe-59 distributions in mice. *J. Nucl. Med.* **1978**, *19*, 930.
(59) Eder, M.; Neels, O.; Muller, M.; Bauder-Wust, U.; Remde, Y.; Schafer, M.; Hennrich, U.; Eisenhut, M.; Afshar-Oromieh, A.; Haberkorn, U.; Kopka, K. Novel Preclinical and Radiopharmaceutical Aspects of [68Ga]Ga-PSMA-HBED-CC: A New PET Tracer for Imaging of Prostate Cancer. *Pharmaceuticals* **2014**, *7*, 779.

DOI: 10.1021/acs.inorgchem.8b01208
Inorg. Chem. XXXX, XXX, XXX−XXX

(60) Sarkar, S.; Bhatt, N.; Ha, Y. S.; Huynh, P. T.; Soni, N.; Lee, W.; Lee, Y. J.; Kim, J. Y.; Pandya, D. N.; An, G. I.; Lee, K. C.; Chang, Y.; Yoo, J. High in Vivo Stability of Cu-64-Labeled Cross-Bridged Chelators Is a Crucial Factor in Improved Tumor Imaging of RGD Peptide Conjugates. *J. Med. Chem.* **2018**, *61*, 385.
(61) Price, E. W.; Zeglis, B. M.; Cawthray, J. F.; Ramogida, C. F.; Ramos, N.; Lewis, J. S.; Adam, M. J.; Orvig, C. H(4)octapa-trastuzumab: versatile acyclic chelate system for 111In and 177Lu imaging and therapy. *J. Am. Chem. Soc.* **2013**, *135*, 12707.
(62) Kim, Y. S.; Wang, F.; Liu, S. Minimizing liver uptake of cationic Tc radiotracers with ether and crown ether functional groups. *World J. Hepatol.* **2010**, *2*, 21.
(63) Liu, S. Ether and crown ether-containing cationic 99mTc complexes useful as radiopharmaceuticals for heart imaging. *Dalton Trans.* **2007**, 1183.
(64) Tsang, B. W.; Mathias, C. J.; Fanwick, P. E.; Green, M. A. Structure-distribution relationships for metal-labeled myocardial imaging agents: comparison of a series of cationic gallium (III) complexes with hexadentate bis(salicylaldimine) ligands. *J. Med. Chem.* **1994**, *37*, 4400.
(65) Thews, O.; Zimny, M.; Eppard, E.; Piel, M.; Bausbacher, N.; Nagel, V.; Rosch, F. In Vitro and In Vivo Structure-Property Relationship of Ga-68-Labeled Schiff Base Derivatives for Functional Myocardial PET Imaging. *Mol. Imaging. Biol.* **2014**, *16*, 802.
(66) Tarkia, M.; Saraste, A.; Saanijoki, T.; Oikonen, V.; Vahasilta, T.; Strandberg, M.; Stark, C.; Tolvanen, T.; Teras, M.; Savunen, T.; Green, M. A.; Knuuti, J.; Roivainen, A. Evaluation of Ga-68-labeled tracers for PET imaging of myocardial perfusion in pigs. *Nucl. Med. Biol.* **2012**, *39*, 715.
(67) Hsiao, Y. M.; Mathias, C. J.; Wey, S. P.; Fanwick, P. E.; Green, M. A. Synthesis and biodistribution of lipophilic and monocationic gallium radiopharmaceuticals derived from N,N ′-bis(3-amino-propyl)-N,N ′-dimethylethylenediamine: potential agents for PET myocardial imaging with Ga-68. *Nucl. Med. Biol.* **2009**, *36*, 39.
(68) van Tilborg, G. A.; Vucic, E.; Strijkers, G. J.; Cormode, D. P.; Mani, V.; Skajaa, T.; Reutelingsperger, C. P.; Fayad, Z. A.; Mulder, W. J.; Nicolay, K. Annexin A5-functionalized bimodal nanoparticles for MRI and fluorescence imaging of atherosclerotic plaques. *Bioconjugate Chem.* **2010**, *21*, 1794.
(69) Thorp-Greenwood, F. L.; Coogan, M. P. Multimodal radio-(PET/SPECT) and fluorescence imaging agents based on metallo-radioisotopes: current applications and prospects for development of new agents. *Dalton Trans.* **2011**, *40*, 6129.
(70) Bullok, K. E.; Dyszlewski, M.; Prior, J. L.; Pica, C. M.; Sharma, V.; Piwnica-Worms, D. Characterization of novel histidine-tagged Tat-peptide complexes dual-labeled with (99m)Tc-tricarbonyl and fluorescein for scintigraphy and fluorescence microscopy. *Bioconjugate Chem.* **2002**, *13*, 1226.
(71) Xu, H.; Baidoo, K.; Gunn, A. J.; Boswell, C. A.; Milenic, D. E.; Choyke, P. L.; Brechbiel, M. W. Design, synthesis, and characterization of a dual modality positron emission tomography and fluorescence imaging agent for monoclonal antibody tumor-targeted imaging. *J. Med. Chem.* **2007**, *50*, 4759.
(72) Esteves, T.; Xavier, C.; Gama, S.; Mendes, F.; Raposinho, P. D.; Marques, F.; Paulo, A.; Pessoa, J. C.; Rino, J.; Viola, G.; Santos, I. Tricarbonyl M(I) (M = Re, (99m)Tc) complexes bearing acridine fluorophores: synthesis, characterization, DNA interaction studies and nuclear targeting. *Org. Biomol. Chem.* **2010**, *8*, 4104.
(73) Bhushan, K. R.; Misra, P.; Liu, F.; Mathur, S.; Lenkinski, R. E.; Frangioni, J. V. Detection of breast cancer microcalcifications using a dual-modality SPECT/NIR fluorescent probe. *J. Am. Chem. Soc.* **2008**, *130*, 17648.
(74) Ramogida, C. F.; Murphy, L.; Cawthray, J. F.; Ross, J. D.; Adam, M. J.; Orvig, C. Novel "bi-modal" H2dedpa derivatives for radio- and fluorescence imaging. *J. Inorg. Biochem.* **2016**, *162*, 253.
(75) Uppal, R.; Ciesienski, K. L.; Chonde, D. B.; Loving, G. S.; Caravan, P. Discrete bimodal probes for thrombus imaging. *J. Am. Chem. Soc.* **2012**, *134*, 10799.
(76) Yanai, T.; Tew, D. P.; Handy, N. C. A new hybrid exchange–correlation functional using the Coulomb-attenuating method (CAM-B3LYP). *Chem. Phys. Lett.* **2004**, *393*, 51.
(77) Scalmani, G.; Frisch, M. J. Continuous surface charge polarizable continuum models of solvation. I. General formalism. *J. Chem. Phys.* **2010**, *132*, 114110.
(78) Wadt, W. R.; Hay, P. J. Ab initio effective core potentials for molecular calculations. Potentials for main group elements Na to Bi. *J. Chem. Phys.* **1985**, *82*, 284.
(79) Adamo, C.; Barone, V. Toward reliable density functional methods without adjustable parameters: The PBE0 model. *J. Chem. Phys.* **1999**, *110*, 6158.
(80) Gran, G. Determination of the equivalence point in potentiometric titrations. Part II. *Analyst* **1952**, *77*, 661.
(81) Paul, M.; Long, F. H0 and related indicator acidity function. *Chem. Rev.* **1957**, *57*, 1.
(82) Baes, C.; Mesmer, R. In *The Hydrolysis of Cations;* John Wiley & Sons: New York, 1976.
(83) Lin, K. S.; Pan, J.; Amouroux, G.; Turashvili, G.; Mesak, F.; Hundal-Jabal, N.; Pourghiasian, M.; Lau, J.; Jenni, S.; Aparicio, S.; Bénard, F. In vivo radioimaging of bradykinin receptor B1, a widely overexpressed molecule in human cancer. *Cancer Res.* **2015**, *75*, 387–393.

DOI: 10.1021/acs.inorgchem.8b01208
Inorg. Chem. XXXX, XXX, XXX–XXX